Journal of Catalysis 270 (2010) 86–94

Contents lists available at ScienceDirect

Journal of Catalysis

journal homepage: www.elsevier.com/locate/jcat

Size- and support-dependent silver cluster catalysis for chemoselective hydrogenation of nitroaromatics

Ken-ichi Shimizu *, Yuji Miyamoto, Atsushi Satsuma

Department of Molecular Design and Engineering, Graduate School of Engineering, Nagoya University, Nagoya 464-8603, Japan

ARTICLE INFO

Article history:
Received 29 October 2009
Revised 8 December 2009
Accepted 9 December 2009
Available online 6 January 2010

Keywords:
Hydrogenation of nitroaromatics
Silver catalysts
Chemoselective hydrogenations
In situ FTIR

ABSTRACT

Silver clusters on θ-Al_2O_3 support catalyze highly chemoselective reduction of a nitro group for the reduction of substituted nitroaromatics such as nitrostyrene. These catalysts show higher selectivity than conventional platinum-group metal-based heterogeneous catalysts. Systematic studies on the influence of the metal particle size and support oxides show that the intrinsic activity increases with decrease in the silver particle size, and acid–base bifunctional supports such as Al_2O_3 give higher activity than acidic or basic supports. Kinetic and in situ infrared studies provide a reaction mechanism which explains fundamental reasons of these tendencies. Cooperation of the acid–base pair site on Al_2O_3 and the coordinatively unsaturated Ag sites on the silver cluster is responsible for the rate-limiting H_2 dissociation to yield a H^+/H^- pair at metal/support interface, while the basic site on oxides acts as an adsorption site of nitroaromatics. High chemoselectivity could be attributed to a preferential transfer of the H^+/H^- pair to the polar bonds in the nitro group.

1. Introduction

Metal clusters have interesting catalytic properties. For example, gold as an inert d^{10} element shows similar or higher catalytic properties for various reactions than platinum-group metal (PGM)-based catalysts when a few nanometer-sized gold is supported on a specific oxide [1–14]. Silver, as a less expensive group IB metal, has been a popular element in a field of nanoparticle synthesis [15]. However, compared with a research on gold nanoparticle catalysis, less attempts [16–34] have been focused on the catalysis of silver clusters or nanoparticles and structure–activity relationship of these catalysts. Our research group reported a series of studies on silver cluster catalysis in the NO*x* selective reduction for automobile application [27], oxidant-free alcohol dehydrogenation [28], hydrogen auto-transfer C—C coupling reaction of alcohols [29], direct dehydrogenative amide synthesis from alcohols and amines [30], and *N*-benzylation of anilines with alcohols [31].

Silver has drawn less attention as a catalyst for hydrogenation [16–26] than PGM catalysts. From theoretical [35–37] and experimental studies, it is well known that hydrogen interacts only very weakly with extended silver surfaces (single crystals, polycrystalline surfaces), and no dissociative chemisorption should occur at low temperature. This was attributed to the completely filled d-band of silver as well as the position of the d-band center relative to the Fermi level [35]. However, a group of Claus first reported excellent selectivity of silver nanoparticle catalysts for the hydrogenation of a C=O group in the presence of a C=C bond [16]. For the selective hydrogenation of crotonaldehyde by TiO_2- or SiO_2-supported silver particles with size of 1–7 nm, the larger silver particles gave higher selectivity to the desired product, unsaturated alcohol [16]. Chen et al. reported that Ag/SiO_2 with silver nanoparticle size of 7–9 nm catalyzed the selective hydrogenation of chloronitrobenzes to their corresponding chloroanilines, though they did not study the effect of silver particle size on the catalytic activity and selectivity [21].

Selective hydrogenation of nitro group in the presence of other reducible functional groups is an important reaction to produce functionalized anilines as industrial intermediates for a variety of specific and fine chemicals [38]. Stoichiometric amount of reducing agents such as iron [39], sodium hydrosulfite [40], tin [41], or zinc in ammonium hydroxide [42] have been successfully used to reduce aromatic nitro compounds containing olefinic bonds. However, these processes produce a large number of by-products. Catalytic hydrogenation by H_2 is more ideal, but conventional PGM catalysts simultaneously hydrogenate both the nitro and olefinic or carbonyl functions. Several catalytic systems for the selective reduction of nitroaromatics have been reported [8,10,11–13,21,38–49]. However, only a few reports [10,11–13,47,48] succeeded in the selective hydrogenation of nitrostyrene. Corma [11–13] succeeded in the selective hydrogenation of nitrostyrene using gold nanoparticles on TiO_2 or Fe_2O_3. They also showed that decoration of the highly active metal (Pt, Ru, and Ni) with the partially reducible support (TiO_2) after pre-reduction at 750 °C resulted in high selectivity

* Corresponding author. Fax: +81 52 789 3193.
E-mail address: kshimizu@apchem.nagoya-u.ac.jp (K.-i. Shimizu).

0021-9517/$ - see front matter © 2009 Elsevier Inc. All rights reserved.
doi:10.1016/j.jcat.2009.12.009

[47]. We recently found that gold nanoparticles on γ-Al_2O_3 catalyze highly chemoselective reduction of a nitro group for the reduction of nitrostyrene [10]. The activity of the gold catalyst depended strongly on the gold size and support oxides, and small Au nanoparticles (2.5 nm) on the acid–base bifunctional support (Al_2O_3) gave highest intrinsic activity [10].

Knowing the fact that silver has lower hydrogenation activity than PGM, we envisioned that the silver catalyst would be applicable to the chemoselective hydrogenation of substituted nitroaromatics to the corresponding anilines. Herein, we report that silver clusters supported on Al_2O_3 selectively catalyze the hydrogenation of nitro group in the presence of C=C, C=O, or C≡N groups. To establish a design concept of silver-based selective hydrogenation catalysts, we show detailed mechanistic and structural studies that address the influence of the silver particle size and the support.

2. Experimental section

2.1. General

The gas chromatography (GC, with Shimadzu GC-17A) and gas chromatography/mass spectrometry (GC/MS, with Shimadzu GCMS-QP5000) were carried out with Rtx-65 or DB-1 capillary column (Shimadzu) using nitrogen as the carrier gas. Commercially available organic and inorganic compounds were used without further purification.

2.2. Catalyst preparation

θ-Al_2O_3 (with surface area of 112 $m^2\ g^{-1}$) and γ-Al_2O_3 (with surface area of 224 $m^2\ g^{-1}$) were prepared by calcination of γ-AlOOH (Catapal B Alumina purchased from Sasol) at 1000 °C and 600 °C for 3 h, respectively. CeO_2 (JRC-CEO-1), TiO_2 (JRC-TIO-4), and MgO (JRC-MGO-1) were supplied from Catalysis Society of Japan. Hydrates of ZrO_2, SnO_2, and WO_3 were prepared by hydrolysis of zirconium oxynitrate 2-hydrate, $SnCl_4{\cdot}6H_2O$, and ammonium paratungstate, respectively, in distilled water by gradually adding an aqueous NH_4OH solution (1.0 mol dm^{-3}), filtration of precipitate, washing with distilled water three times, and dryness at 100 °C. Sepiolite (Konan, China), a fibrous natural clay mineral with ideal formula of $Mg_8Si_{12}O_{30}(OH)_4{\cdot}4H_2O{\cdot}nH_2O$, was treated with dilute HCl aqueous solution (0.59 mol dm^{-3}) to eliminate impurities (calcite and dolomite). Supported silver catalysts were prepared by impregnating support oxides with an aqueous solution of silver nitrate followed by evaporation to dryness at 80 °C, calcination in air at 500 or 600 °C for 3 h, and reduction in a flow of H_2 at 100–900 °C for 10 min. Ag content, calcination temperature, and H_2-reduction temperature are summarized in Table 1. The catalysts are designated as Ag/support-*x*, where *x* is the average particle size (nm) of metallic Ag species estimated from the extended X-ray absorption fine structure (EXAFS) or XRD (X-ray diffraction) analyses. Pt/Al_2O_3-1.3 (Pt = 1 wt.%) was prepared by impregnating γ-Al_2O_3 with an aqueous solution of metal nitrate, followed by drying at 80 °C for 12 h, calcining at 500 °C for 2 h, and reducing at 300 °C for 0.5 h in H_2. The average particle size of Pt (1.3 nm) was estimated with the CO uptake of the Pt/Al_2O_3-1.3 at 25 °C using the pulse-adsorption of CO in a flow of He. The Pt particle diameter was estimated assuming that one CO molecule adsorbed onto each Pt atom on the surface of hemispherical Pt particles. The World Gold Council (WGC) test catalyst, Au/TiO_2 (Au = 3 wt.%), was purchased from the WGC. Commercial PGM-based heterogeneous catalysts, Rh/Al_2O_3 (Rh = 5 wt.%, AA-3501), Ru/Al_2O_3 (Ru = 5 wt.%, AA-4501), Pd/C (Pd = 5 wt.%, AC-2500), and Pd/Al_2O_3 (Pd = 5 wt.%, AA-2501) were kindly supplied from N.E. Chemcat Corporation.

Table 1
List of the catalysts.

Catalysts-*x*[a]	Supports	Ag (wt.%)	T_{cal} (°C)[b]	T_H (°C)[c]	*S* ($m^2\ g^{-1}$)[d]
Ag/MgO-3.0	MgO	5	500	100	57
Ag/CeO_2-0.9	CeO_2	5	500	100	61
Ag/ZrO_2-1.6	ZrO_2	5	500	100	69
Ag/sepiolite-1.6	Sepiolite	5	500	500	189
Ag/TiO_2-1.3	TiO_2	5	500	100	36
Ag/SnO_2-1.6	SnO_2	5	500	500	42
Ag/WO_3-1.6	WO_3	5	500	500	5.8
Ag/Al_2O_3-0.7	θ-Al_2O_3	1	600	500	107
Ag/Al_2O_3-0.9	θ-Al_2O_3	5	600	300	105
Ag/Al_2O_3-l.l	θ-Al_2O_3	5	600	500	105
Ag/Al_2O_3-3.4	θ-Al_2O_3	5	600	700	104
Ag/Al_2O_3-25	θ-Al_2O_3	5	600	900	104

[a] Average particle size (nm) of metallic Ag species estimated from EXAFS or XRD analyses.
[b] Calcination temperature.
[c] Temperature of H_2-reduction after calcination.
[d] Specific surface area of the catalyst determined by N_2 adsorption.

2.3. XAFS

Ag K-edge EXAFS measurements were performed in transmission mode at the BL01B1 in the SPring-8. The storage ring was operated at 8 GeV. A Si(1 1 1) single crystal was used to obtain a monochromatic X-ray beam. Samples were sealed in cells made of polyethylene under ambient atmosphere, and XAFS spectra were taken at room temperature. The EXAFS analysis was performed using the REX version 2.5 program (RIGAKU). The Fourier transformation of the k^3-weighted EXAFS oscillation from *k*-space to *r*-space was performed over the range 40–140 nm^{-1} to obtain a radial distribution function. The inversely Fourier-filtered data (in a range 0.15–0.32 nm) were analyzed with a usual curve-fitting method in *k*-space in a range of 40–140 nm^{-1}. For the curve-fitting analysis, the empirical phase shift and amplitude functions for Ag–Ag and Ag–O shells were extracted from the data for Ag foil and Ag_2O, respectively.

2.4. HAADF-STEM

High-angle annular dark field scanning TEM (HAADF-STEM) image was recorded using a HD-2300S (Hitachi) microscope operated at 200 kV. Fig. 1 shows representative HAADF-STEM images of Ag/Al_2O_3-0.9. Nearly spherical Ag particles with size in a range 0.8–4.2 nm are observed. However, particle size determination of this sample was unsuccessful, because contrast between Al_2O_3 and silver was quite low especially for silver cluster size with diameter below 0.8 nm. In addition, during the HAADF-STEM observation of Ag/Al_2O_3-0.9, bright points due to silver clusters with diameter below 1 nm disappeared possibly due to the reaction of silver cluster with carbonaceous residue under a strong electron beam irradiation. Therefore, in this study, the mean diameter of silver particles was not estimated from TEM, but from XRD (for Ag/Al_2O_3-25) or EXAFS (for other silver catalysts).

2.5. In situ FTIR

In situ FTIR, spectra were recorded on a JASCO FT/IR-620 equipped with a quartz IR cell connected to a conventional flow reaction system. The sample was pressed into a 20 mg of self-supporting wafer and mounted into the quartz IR cell with CaF_2 windows. Spectra were measured accumulating 5–20 scans at a resolution of 4 cm^{-1}. A reference spectrum of the catalyst wafer in He taken at measurement temperature was subtracted from each spectrum. Prior to each experiment, the catalyst disk was heated in He flow (100 $cm^3\ min^{-1}$) at 500 °C for 0.5 h, followed

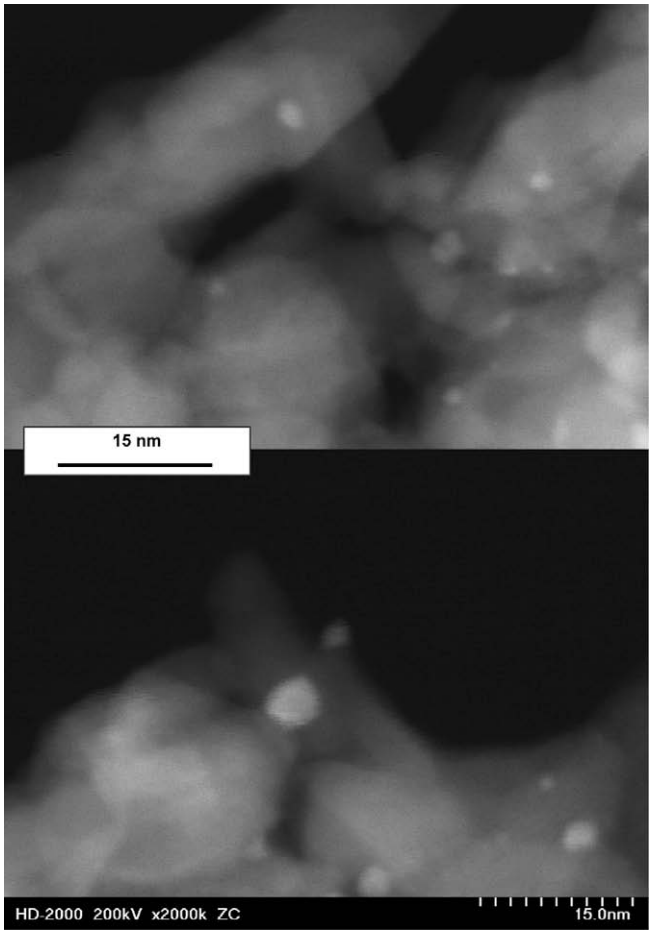

Fig. 1. HAADF-STEM images of Ag/Al_2O_3-0.9.

by the H_2-reduction at the temperature shown in Table 1, and by cooling to the desired temperature under He flow. For the introduction of nitro compounds to the IR disc, the liquid compound was injected under a He flow preheated at 120 °C which was fed to the in situ IR cell. Then, the IR disk was purged with He for 600 s.

2.6. Typical procedures for the catalytic test

Catalytic experiments of chemoselective hydrogenation of nitro compounds were carried out in a 30-cm^3 autoclave with a glass tube inside equipped with magnetic stirring. In each reaction, 2 mmol substrate and 15-cm^3 tetrahydrofuran as solvent were placed into the autoclave together with typically 0.1 g catalyst. After being sealed, the reactors were flushed with H_2 and then pressurized at 3.0 MPa, and then heated to the required temperature (typically 160 °C). Conversion and yield of products were determined by GC using *n*-dodecane as an internal standard. The products were identified by GC–MS (GCMS-QP5000, Shimazu) equipped with the same column and in the same conditions as GC and also by comparison with commercially pure products.

3. Results and discussion

3.1. Characterization of catalysts

We prepared a series of supported silver catalysts with the same silver content (5 wt.%) and similar silver particle size but with a variety of supports (θ-Al_2O_3, CeO_2, MgO, ZrO_2, sepiolite, TiO_2, SnO_2, WO_3). Details on the preparation method are summarized in Table 1. Ag K-edge EXAFS of all the samples (Fig. 2, Table 2) consist of a Ag–Ag contribution with a negligible Ag–O contribution, indicating that metallic silver species are the dominant silver species in all samples. The catalysts are designated as Ag/support-*x*, where *x* is the average particle size (nm) of metallic silver species determined by EXAFS or XRD as shown in the following paragraphs. For Al_2O_3 supported catalysts, a series of catalysts with average silver particle diameter from 0.7 to 25 nm were also prepared by changing the Ag content (1 or 5 wt.%) and H_2-reduction temperature (300–900 °C); the particle diameter increased with Ag content and H_2-reduction temperature. For the Ag/Al_2O_3-25 sample, an intense XRD line due to the Ag(1 1 1) reflection ($2\theta = 38.1°$) was observed, and the average particle size was estimated from the line broadening using Scherrer equation. EXAFS analysis in Table 2 shows that the Ag–Ag coordination numbers (6.2–10.7) are much lower than that of the bulk silver (12) except for Ag/Al_2O_3-25, which indicates that silver species in these samples are small metal particles or metal clusters. Following the method by Jentys [50], average size of metallic silver was determined using the Ag–Ag coordination number. Note that Jentys confirmed that the shape of the particles has minor influence on the metal particle size; the differences in the size are within the typical limits of accuracy in the EXAFS coordination numbers (±10%) [50].

3.2. Catalytic properties

It has been already shown by Corma et al. that hydrogenation of nitrostyrene by Pt- or Pd-based conventional hydrogenation catalysts results in non-chemoselective reduction to ethylaniline rather than selective reduction to aminostyrene [13,47]. For example, 5%Pt/C showed 29% and 63% selectivities to aminostyrene and ethylaniline, respectively, at 96% conversion at 40 °C [47]. Thus, selective reduction of 4-nitrostyrene to 4-aminostyrene was chosen as the model reaction (Table 3). Pt/Al_2O_3-1.3 as a conventional hydrogenation catalyst showed 100% selectivity to the undesirable by-product (4-ethylaniline, **3**). Other commercial PGM-based catalysts with metal loading of 5 wt.% (Rh/Al_2O_3, Ru/Al_2O_3, Pd/Al_2O_3, and Pd/C) also showed 100% selectivity to the by-product **3** (result

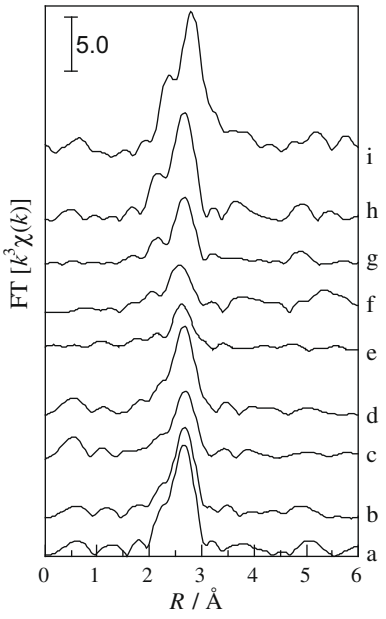

Fig. 2. Ag K-edge EXAFS Fourier transforms of representative samples: (a) Ag/WO_3-2.6, (b) Ag/SnO_2-2.4, (c) Ag/TiO_2-1.3, (d) Ag/sepiolite-2.6, (e) Ag/Al_2O_3-1.1, (f) Ag/ZrO_2-1.7, (g) Ag/CeO_2-0.9, (h) Ag/MgO-3.0, and (i) Ag foil.

Table 2
Ag K-edge EXAFS analysis of various catalysts.

Catalysts-x[a]	Shell	CN[b]	R (Å)[c]	σ^2 (Å^2)[d]	R_f (%)[e]
Ag/MgO-3.0	Ag	10.0	2.89	0.060	1.7
Ag/CeO_2-0.9	Ag	6.2	2.88	0.068	3.1
Ag/ZrO_2-1.6	Ag	8.5	2.89	0.069	1.8
Ag/sepiolite-1.6	Ag	10.5	2.89	0.069	0.9
Ag/TiO_2-1.3	Ag	7.9	2.90	0.068	3.6
Ag/SnO_2-1.6	Ag	7.9	2.90	0.068	3.6
Ag/WO_3-1.6	Ag	9.7	2.89	0.053	2.4
Ag/Al_2O_3-0.7	Ag	6.1	2.86	0.104	1.9
	O	0.3	1.97	0.073	
Ag/Al_2O_3-3.4	Ag	9.5	2.89	0.062	3.0
Ag/Al_2O_3-l.l	Ag	7.1	2.87	0.084	3.2
Ag/Al_2O_3-25	Ag	11.4	2.89	0.062	0.7

[a] Average particle size of metallic Ag from the EXAFS or XRD analyses.
[b] Coordination numbers.
[c] Bond distance.
[d] Debye–Waller factor.
[e] Residual factor.

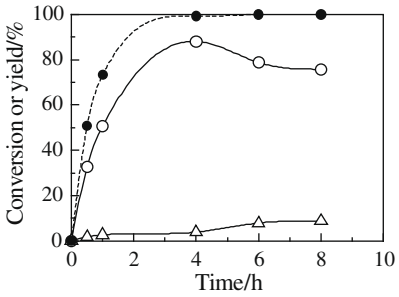

Fig. 3. Yields of (○) 4-aminostyrene and (Δ) 3-ethylaniline and (●) conversion of 4-nitrostyrene for 4-nitrostyrene hydrogenation with Ag/Al_2O_3-0.7 (0.13 mol%) at 160 °C.

not shown). In contrast, most of the silver catalysts produced 4-aminostyrene **2** as a main product and much less amount of **3**. A typical time-course of the reaction products in the presence of Ag/Al_2O_3-0.7 is shown in Fig. 3. The GC/MS experiment showed that only **3** was a detectable by-product, but hydroxylamine, styrene, azostyrene, and azoxystyrene were not detected. Among the silver catalysts in Table 3,

Ag/Al_2O_3-0.9 showed excellent selectivity (>96%) at 100% conversion. Table 3 also lists the initial rate of 4-aminostyrene formation measured under the condition where conversion was below 40%. Note that for the catalyst with high activity, the rates were determined in separate catalytic experiments using small amount of catalyst (0.04 mol% with respect to 4-nitrostyrene). The selectivity for **2** did not markedly depend on the support material except for MgO. In contrast, the reaction rate depended on the nature of the support material. Among a series of silver cluster catalysts supported on various metal oxides, Ag/Al_2O_3-0.9 showed the highest rate per gram of the catalyst. The reaction rate and selectivity of Ag/Al_2O_3-0.9 were close to those of Au/TiO_2 supplied from the WGC.

The Ag/Al_2O_3-0.9 catalyst can be easily separated from the reaction mixture by a centrifugation. The separated Ag/Al_2O_3-0.9 was washed with ethanol (5 mL) and distilled water (5 mL), followed by drying at 100 °C for 30 min and calcining in air at 700 °C for 10 min, and by reducing in H_2 at 300 °C for 5 min. The recovered catalyst showed high conversion and slightly less selectivity than the first run (Table 4). To estimate the reaction rate in the second cycle, we performed an additional catalyst recycle test using small amount of Ag/Al_2O_3-0.9 (0.04 mol%) after the first catalytic run. The initial rate, measured under the condition where conversion was below 40%, decreased from 85 to 62 mmol h^{-1} g^{-1} (result not shown).

Table 3
Hydrogenation of 4-nitrostyrene by various catalysts.[a]

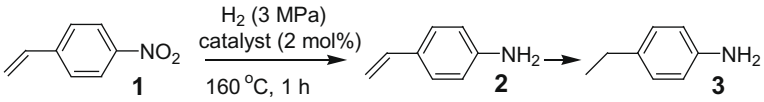

Entry	Catalysts-x[b]	Conv. (%)	Selectivity		V (mmol h^{-1} g^{-1})
			2	**3**	
1	Ag/Al_2O_3-0.7[c]	99	88	3.9	46[d]
2	Ag/Al_2O_3-0.9	100	96	3.0	85[d]
3	Ag/Al_2O_3-l.l	100	95	2.9	45[d]
4	Ag/Al_2O_3-3.4	31	73	2.6	5.2
5	Ag/Al_2O_3-25	31	0	0	0
6	Ag/WO_3-2.6	11	98	0	5.9
7	Ag/SnO_2-2.4	3	79	0	1.0
8	Ag/TiO_2-1.3	100	92	1.4	30[d]
9	Ag/sepiolite-3.7	100	89	1.4	8.9[d]
10	Ag/ZrO_2-1.6	61	73	3.0	8.9[d]
11	Ag/CeO_2-0.9	59	74	0	8.7
12	Ag/MgO-3.0	3	21	0	0.15
13	Ag powder[e]	1	0	0	0
14	Pt/Al_2O_3-1.3[d]	100	0	100	0
15	Pt/Al_2O_3-1.3[f]	45	0	65	0
16	Au/TiO_2[d,g]	100	95	0.5	76

[a] 4-Nitrostyrene (2 mmol), THF (15 mL), Ag loading = 5 wt.% (2 mol% with respect to 4-nitrostyrene). Conversion of **1** and selectivities of **2** and **3** were determined by GC. Initial rate of 4-aminostyrene formation (V) was measured under the condition where conversion was below 40%.
[b] Average particle size of Ag (nm).
[c] Ag loading = 1 wt.% (0.13 mol% with respect to 4-nitrostyrene).
[d] Catalyst = 0.04 mol%.
[e] Catalyst = 40 mol%.
[f] T = 70 °C, t = 1 h, catalyst = 0.04 mol%.
[g] Standard catalyst with Au loading of 3 wt.% supplied from WGC.

Table 4
Selective hydrogenation of nitroaromatic compounds.[a]

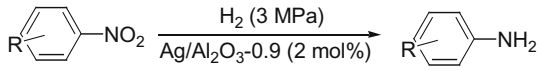

Entry	R	*t* (h)	Conv. (%)	Selectivity (%)[b]
1	4-Vinyl	1	100	96 (3)
2[c]	4-Vinyl	1	100	91 (8)
3	3-Vinyl	1	100	92 (4)
4[d]	4-$COCH_3$	20	100	97 (0)
5	4-CN	20	100	86 (0)
6[e]	4-$CONH_2$	20	100	92 (0)

[a] Substrate (2 mmol), THF (15 mL), T = 160 °C, t = 1 h.
[b] Selectivity of by-products in which R groups are also reduced are shown in parentheses.
[c] Second cycle.
[d] Ag = 0.2 mol%.
[e] Ag = 0.8 mol%.

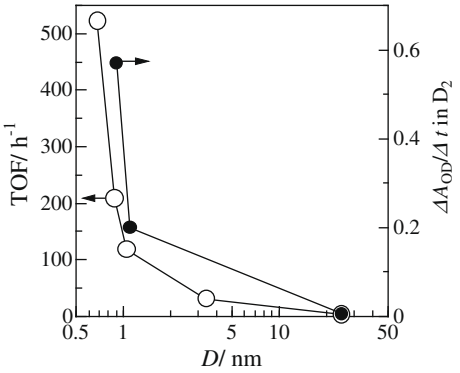

Fig. 4. (○) TOF based on the number of surface Ag atom for 4-nitrostyrene hydrogenation and (●) initial rate of OH/D_2 isotope exchange as a function of Ag particle size in Ag/Al_2O_3.

With suitable catalysts, Ag/Al_2O_3-0.9, hydrogenation of a series of nitroaromatic compounds with alkene, carbonyl, nitrile, and amide groups was tested to investigate the scope of the reaction (Table 4). Good to excellent selectivities (86–97%) at 100% conversions were obtained in hydrogenation of these substrates. In the products, there were small amount of by-products in which the substituent groups were also reduced, but there were no other GC/MS-detectable by-products.

3.3. Structure–activity relationship

Systematic catalytic and spectroscopic studies on the influence of the silver particle size in Ag/Al_2O_3 show the nature of active silver species. By using the mean diameter of metallic silver and the atomic diameter of silver (0.289 nm) and assuming that the supported silver clusters can be modeled as a fcc crystal lattice, the number of surface silver atoms for each catalyst can be statistically determined according to the established method [3]. For a series of Ag/Al_2O_3 catalysts with different silver particle sizes, the initial rate of 4-aminostyrene formation per gram of the Ag/Al_2O_3 catalyst (V) was measured under the condition where conversion was below 40% (Table 3), and the turnover frequency (TOF) per surface Ag sites was estimated. The TOF is plotted as a function of the average particle size in Fig. 4. Clearly, the silver cluster with smaller particle size gives higher intrinsic activity, indicating that the present reaction is a structure-sensitive reaction demanding coordinatively unsaturated Ag site.

To investigate the effect of acid–base characteristics of support material, the TOF are plotted in Fig. 5 as a function of the electronegativity of metal oxide, which has been used, to a first approximation, as a parameter of acidity (or electrophilicity) of metal oxides [51]. The result shows that the support with strong basic character (CeO_2 and MgO) and that with acidic character (SnO_2 and WO_3) resulted in low activity. This suggests that both acidic and basic surface sites are necessary for this reaction.

We recently reported structure–activity relationship in gold-catalyzed chemoselective reduction of a nitro group for the reduction of substituted nitroaromatics. It was found that the activity of gold catalyst depended on the gold size and support oxides; smaller Au nanoparticles on the acid–base bifunctional support (Al_2O_3) gave highest intrinsic activity [10]. These tendencies are very similar to those observed for the silver-catalyzed chemoselective reduction of a nitro group found in the present study, which may suggest similar mechanistic reasons affecting the activity of group IB metal-based catalysts for this reaction.

3.4. Reaction mechanism

To establish the reaction pathway, we studied the hydrogenation of nitrobenzene by in situ FTIR spectroscopy measured at each temperature under a flow of He or H_2 (normal pressure). When nitrobenzene is adsorbed on the Al_2O_3 support or on the Ag/Al_2O_3-0.9 catalyst at 80 °C (Fig. 6), the asymmetric $\nu_{as}(NO_2)$ IR vibration frequency shifts from 1552 cm^{-1} in the gas phase to 1526 cm^{-1}, while very small shifts for the aromatic ring vibration frequencies (1617, 1602, 1583 cm^{-1}) are observed. The $\nu_{as}(NO_2)$ band for nitrobenzene on θ-Al_2O_3 appeared at 1526 cm^{-1} (Fig. 6). These results suggest that nitrobenzene interacts with the catalyst surface through the nitro group. Reactivity of the nitrobenzene adspecies ($PhNO_{2\ ad}$) was studied by time-resolved in site IR (Fig. 7) measured at 80 °C. The intensity of the band at 1350 cm^{-1} due to the symmetric $\nu_s(NO_2)$ of $PhNO_{2\ ad}$ on Ag/Al_2O_3-0.9 did not decrease under a flow of He. When the flowing gas was switched to H_2, the band due to $PhNO_{2\ ad}$ disappeared at t = 180 s. Simultaneously, a band assignable to phenylhydroxylamine (PhNHOH) at 1455 cm^{-1} appeared and gradually disappeared after 120 s. Then, new bands due to adsorbed aniline (1500, 1605 cm^{-1}) appeared

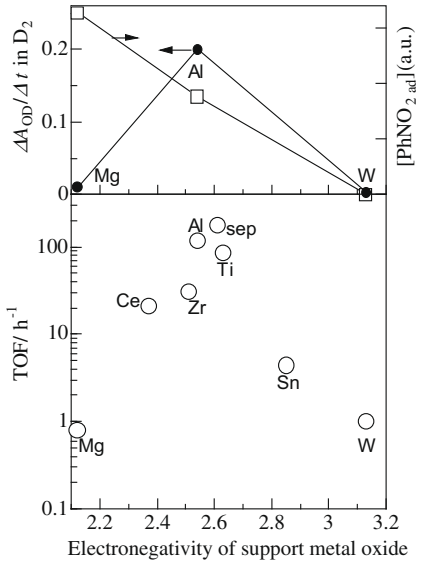

Fig. 5. (○) TOF based on the number of surface Ag atom for 4-aminostyrene formation (from entries 3, 6–12 in Table 3), (●) initial rate of OH/D_2 isotope exchange (from Fig. 10), and (□) relative amount of $PhNO_{2\ ad}$ (from Fig. 6) as a function of the electronegativity of support oxide.

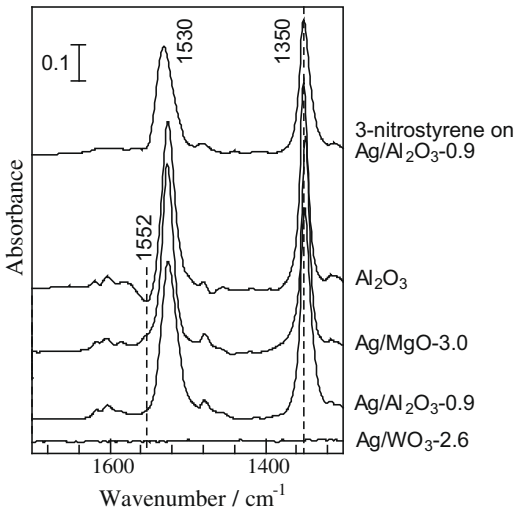

Fig. 6. FTIR spectra of adsorbed species on various catalysts taken at 80 °C after introducing nitrobenzene (1.0 mmol g^{-1}), followed by purging with He for 600 s.

and their intensities increased with time. In contrast, $PhNO_{2\ ad}$ on Al_2O_3 did not react under the same condition (not shown). These results indicate that the hydrogenation of $PhNO_{2\ ad}$ occurs through the consecutive route via the hydroxylamine intermediate [12,52], and silver cluster plays an important role in the H_2 activation step (Scheme 1).

Kinetic isotope effect in the hydrogenation of $PhNO_{2\ ad}$ under H_2 and D_2 at 100 °C over Ag/Al_2O_3-0.9 was studied by time-resolved in situ IR. Kinetic analysis of the consumption of $PhNO_{2\ ad}$ is shown in Fig. 8. The relative amount of $PhNO_{2\ ad}$ was estimated from the changes in the area of the IR band at 1350 cm^{-1}, because the band had the least overlap with other bands and, therefore, was suitable for the quantitative analysis. The first-order plot for the reduction of $PhNO_{2ad}$ gave fairly good straight line. The first-order rate constants for the reduction of $PhNO_{2\ ad}$ under H_2 and D_2 were estimated to be 4.3×10^{-2} and 7.5×10^{-3} s^{-1}, respectively. The kinetic isotope effect (k_H/k_D) at 100 °C was estimated to be 5.7. The dependence of the rate constant for the reduction of $PhNO_{2\ ad}$ on the hydrogen partial pressure was examined at 80 °C by changing the H_2 concentration of H_2/He mixture. From the slop of the line in Fig. 9, the reaction order with respect to H_2 was estimated to be 0.6. On the other hand, the kinetic experiments for the overall liquid phase hydrogenation of nitrobenzene in THF with Ag/Al_2O_3-0.9 under 3 MPa H_2 showed nearly zero order dependence on the nitrobenzene concentration (result not shown). These results suggest that the cleavage of the H–H bond is the rate-determining step. Previously, Gelder et al. [52] studied the kinetic isotope effect for the liquid phase hydrogenation of nitrobenzene to aniline with palladium/carbon catalyst under high pressure and showed that H–H bond cleavage is the rate-limiting step.

As reported by Claus et al. for Ag/SiO_2 catalyst [19], the isotopic exchange of OH groups of oxide supports to OD groups in D_2 begins with the cleavage of D_2, and thus, this reaction can be considered a model reaction for measuring the rate of H_2 cleavage step. Fig. 10A

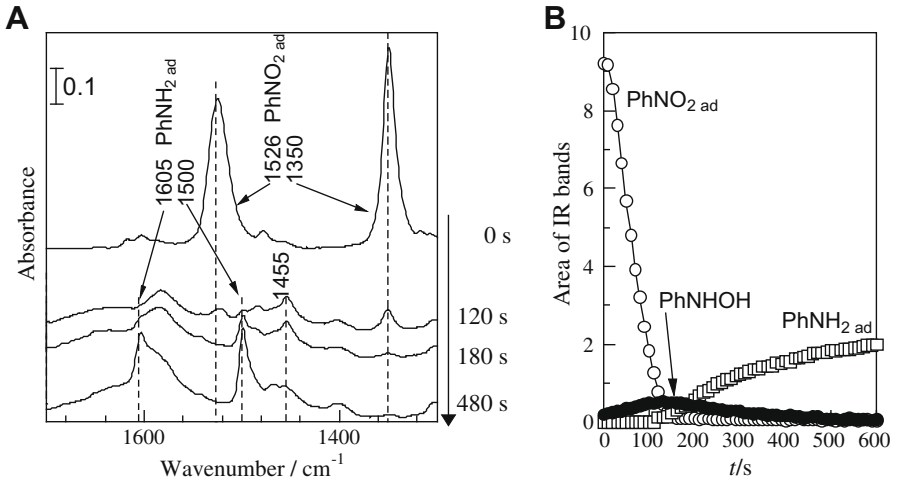

Fig. 7. (A) FTIR spectra of adsorbed species on Ag/Al_2O_3-0.9 at 80 °C as a function of time in a flow of H_2. Before the measurement (t = 0 s), nitrobenzene (1.0 mmol g^{-1}) was introduced to the catalyst disc, followed by purging with He for 600 s. (B) Time-course of the area of the bands due to $PhNO_{2\ ad}$ (○, 1350 cm^{-1}), PhNHOH (●, 1455 cm^{-1}), and $PhNH_{2\ ad}$ (□, 1605 cm^{-1}).

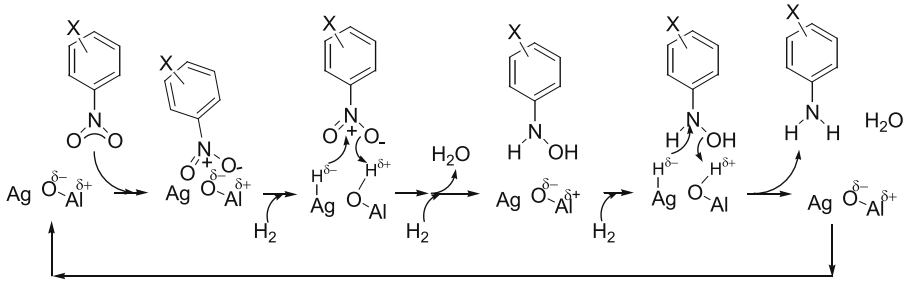

Scheme 1. Proposed mechanism for the Ag/Al_2O_3-catalyzed hydrogenation of nitroaromatic compound.

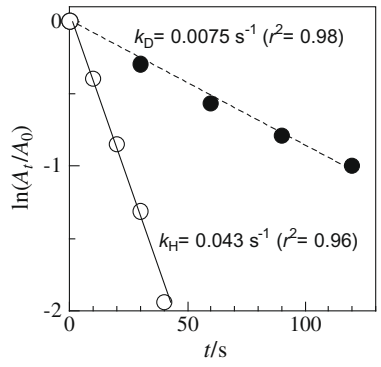

Fig. 8. Isotopic effect in the reduction of $PhNO_{2\ ad}$ on Ag/Al_2O_3-0.9 at 100 °C. The first-order rate constants for $PhNO_{2\ ad}$ reduction under (○) H_2 and (●) D_2 estimated from the changes in the area of the IR band at 1350 cm^{-1} were 4.3×10^{-2} and 7.5×10^{-3} s^{-1}, respectively.

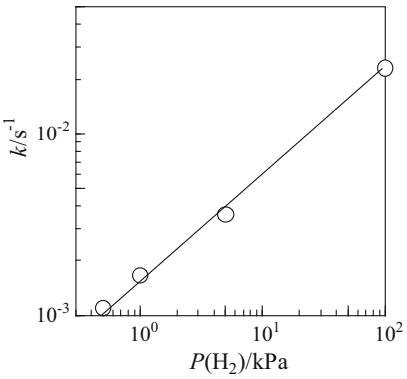

Fig. 9. Effect of hydrogen partial pressure on the first-order rate constant for the reduction of $PhNO_{2\ ad}$ on Ag/Al_2O_3-0.9 at 80 °C under a flow of H_2/He of various H_2 concentration. The rate constant was estimated from the changes in the area of the IR band at 1350 cm^{-1}.

shows the IR spectrum obtained after flowing D_2 for 600 s to Ag/Al_2O_3-0.9 at 150 °C. Loss and gain of IR band intensity in the AlO–H (3100–3800 cm^{-1}) and in the AlO–D (1900–2800 cm^{-1}) stretching regions were observed. Kinetic curves for the OD formation are shown in Fig. 10B. The initial rate of the OD formation on Ag/Al_2O_3-0.9 was more than 500 times higher than that on Al_2O_3, which gave a direct evidence on the silver cluster-catalyzed H–H cleavage.

3.5. Origin of the size- and support-specific silver catalysis

To obtain mechanistic reasons of the size- and support-dependent activity, kinetic curves for the OH/D_2 exchange reaction at 150 °C monitored by in situ IR for various catalysts were compared in Fig. 10, and the initial rates were estimated from the slope of the curve. For Ag/Al_2O_3 with the same Ag loading (5 wt.%) but with different mean Ag particle sizes, the relative exchange rate increased when Ag particle size decreased from 25 to 0.9 nm (Fig. 4). This trend is consistent with the change in the intrinsic rate for the selective 4-nitrostyrene hydrogenation. Taking into account the fact that no dissociative chemisorption of H_2 occurs on the surface of polycrystalline or single crystal silver surface at low temperature, coordinatively unsaturated sites on silver cluster are required for the H_2 dissociation as the rate-determining for the catalytic reduction of nitroaromatics. The effect of support oxide on the rate of OH/D_2 exchange reaction was also examined. For the catalysts with the same Ag loading (5 wt.%) and similar mean Ag particle sizes, the OH/D_2 exchange reaction rate changes in the order of $Al_2O_3 \gg MgO > WO_3$. This suggests that the rate of D_2 dissociation is significantly higher for acid–base bifunctional support (Al_2O_3) than acidic (WO_3) or basic (MgO) support and the acid–base pair site is also required for the H_2 dissociation step.

On the other hand, the surface basic site plays an important role in the adsorption of nitroaromatics. For silver catalysts with the same Ag loading (5 wt.%) and similar mean Ag particle sizes, the relative density of $PhNO_{2\ ad}$ was estimated from IR intensity of the $PhNO_{2\ ad}$ band (1350 cm^{-1}) in Fig. 6 and the surface area of the catalyst (Table 1). As shown in Fig. 5, the relative density of $PhNO_{2\ ad}$ per surface area of the catalyst changes in the order of $MgO > Al_2O_3 \gg WO_3$, which is consistent with the order of basicity of the support. From the earlier discussions, fundamental reasons why both acidic and basic sites are necessary for the title reaction are presented as follows; the acid–base pair site is required for the H_2 dissociation step, and the basic site acts as an adsorption site of nitroaromatics.

3.6. Origin of the chemoselectivity

Finally, the origin of the chemoselectivity is investigated with in situ IR and kinetic experiments. The IR spectrum of 3-nitrosty-

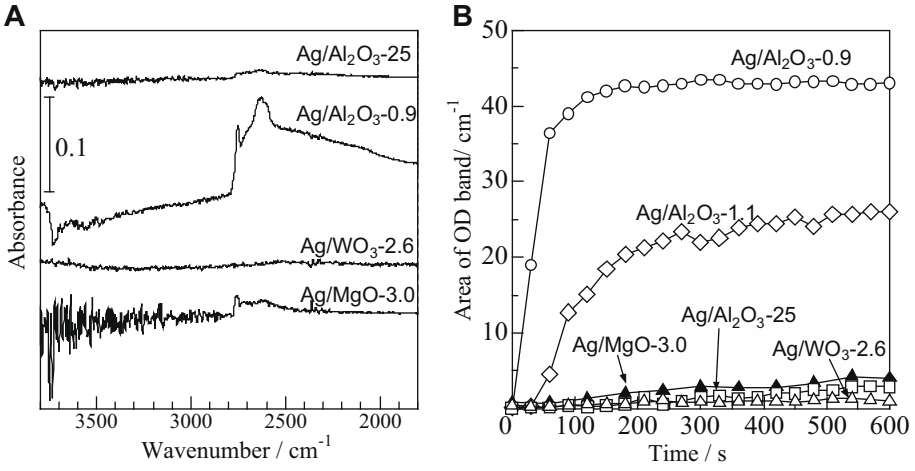

Fig. 10. HD exchange of surface OH groups of the catalysts at 150 °C in a flow of D_2. (A) difference IR spectra which were obtained by subtraction of the spectra before the D_2 admission to the sample under He flow (100 cm^3 min^{-1}) from those recorded under D_2 flow (20 cm^3 min^{-1}, t = 600 s). (B) Area of OD band vs. reaction time.

Table 5
Initial rates for hydrogenation of nitrobenzene (V_N) or styrene (V_S).[a]

Catalyst	T (°C)	V_N (mmol g^{-1} h^{-1})	V_S (mmol g^{-1} h^{-1})	V_N/V_S
Ag/Al_2O_3-l.l	120	47	3.6	13
Ag/MgO-3.0	160	7.6	1.4	5.4
Pt/Al_2O_3-1.3	40	27	77	0.35

[a] Substrate (2 mmol), THF (15 mL), H_2 (3 MPa), catalyst (0.1 mol%).

rene adsorbed on Ag/Al_2O_3-0.9 (Fig. 6) shows the bands at 1530 ($\nu_{as}(NO_2)$) and 1350 cm^{-1} ($\nu_s(NO_2)$). The $\nu_{as}(NO_2)$ band with similar position was observed for TiO_2 and Au/TiO_2 (1532 cm^{-1}) and was assigned to the nitrostyrene interacting with the oxide surface through the nitro group [13]. The $\nu_{as}(NO_2)$ band for nitrobenzene on θ-Al_2O_3 appeared at 1530 cm^{-1} (result not shown). Hence, one of the reason of the chemoselective hydrogenation of the nitro group in nitrostyrene could be the preferential adsorption of nitrostyrene through the nitro group on Ag/Al_2O_3.

A more important origin of the selectivity is the higher intrinsic rate for the reduction of the nitro group than that of the olefinic group. Table 5 compares the initial rates for hydrogenations of nitrobenzene and styrene. For Ag/Al_2O_3-1.1, the rate for hydrogenation of nitrobenzene (V_N) is 13 times higher than those for styrene (V_S). In contrast, Pt/Al_2O_3-1.3 exhibits higher activity for styrene (V_N/V_S = 0.35). For the chemoselective hydrogenation of polar bonds (C=O or C=N) with homogeneous metal–ligand bifunctional catalysts, it is widely accepted that the reaction begins with heterolytic cleavage of H_2 to yield H^+ in a OH or NH ligand and H^- in metal hydrides, and the H^+/H^- pair preferentially transfers to the polar bonds [53]. On the other hand, it is established that H_2 addition to solid acid-supported metal catalysts, such as Pt/SO_4^{2-}-ZrO_2, results in the formation of acidic OH groups on the support [54]. Adopting these models, a cooperative mechanism catalyzed by low coordinated Ag atoms and acid–base pair site of Al_2O_3 for the hydrogenation of a nitro group can be proposed as follows. The dissociation of H_2 at silver-support interface yields a $H^{\delta-}$ atom on the low coordinated Ag atom and a H atom which releases an electron to Lewis acid site of the support. The latter species becomes a proton stabilized at the oxygen atom (Lewis base) nearby the Lewis acid site. The electrophilic $H^{\delta+}$ species on the support and nucleophilic $H^{\delta-}$ species on Ag atom transfer to the polar nitro group to yield a hydroxylamine intermediate. The hydroxylamine intermediate then undergoes H^+/H^- transfer to yield the final product (Scheme 1). Important roles of the interface between the support oxide and the metal surface atoms have been proposed in the literature, but most of them have been focused on the reducible character of semiconductor oxides such as TiO_2. For the selective hydrogenation of *p*-chloronitrobenzene with Pt/TiO_2 catalyst, Coq et al. [49] proposed that the suboxide TiO*x* migrating on the Pt particles is responsible for promoting the Pt properties for this reaction, because these ad-species polarize the N=O bond which becomes more susceptible to hydrogen attack. For selective hydrogenation of nitrostyrene by Au/TiO_2, Corma et al. showed that the high chemoselectiviy of the Au/TiO_2 can be attributed to a cooperation between the gold nanoparticle and the support that preferentially activates the nitro group [13]. In their recent quantum chemical study of H_2 activation by Au nanoparticles, they showed that the TiO_2 support plays an important role in the H_2 dissociation; interaction of Au with the reduced TiO_2 surface causes noticeable changes in the shape of the gold nanoparticles and consequently increases the number of potentially active Au sites for H_2 dissociation [14]. In contrast to these proposals, we found that acid–base properties of non-reducible oxide support play an important role in H_2 dissociation as well as the preferential adsorption of substituted nitroaromatics through the nitro group on the catalyst.

4. Conclusions

Silver clusters on θ-Al_2O_3 catalyze highly chemoselective reduction of a nitro group for the reduction of substituted nitroaromatics. Cooperation of the acid–base pair site on Al_2O_3 and the coordinatively unsaturated Ag sites on the silver cluster is responsible for the rate-limiting H_2 dissociation to yield a H^+/H^- pair at metal/support interface, while the basic site on Al_2O_3 acts as an adsorption site of nitroaromatics. High chemoselectivity can be attributed to a preferential transfer of H^+/H^- to the polar bonds in the nitro group. These fundamental aspects are very close to those for Al_2O_3-supported gold nanoparticle catalyst, which has been shown to be effective for the title reaction in our previous study [10]. Hence, the earlier mentioned concept will provide a strategy to design d^{10} metal-based selective hydrogenation catalysts.

Acknowledgments

This work was partly supported by a Grant-in-Aid for Scientific Research B (20360361) from the Japan Society for the Promotion Science. The X-ray absorption experiment was performed with the approval of the Japan Synchrotron Radiation Research Institute (Proposal No. 2008A1633).

References

[1] M. Haruta, Catal. Today 36 (1997) 153.
[2] A. Corma, H. Garcia, Chem. Soc. Rev. 37 (2008) 2096.
[3] A. Abad, A. Corma, H. Garcia, Chem. Eur. J. 14 (2008) 212.
[4] D.P. He, H. Shi, Y. Wu, B.Q. Xu, Green Chem. 9 (2007) 849.
[5] L. Liu, B. Qiao, Y. Ma, J. Zhang, Y. Deng, Dalton Trans. (2008) 2542.
[6] Y. Chen, J. Qiu, J.X. Wang, J. Xiu, J. Catal. 242 (2006) 227.
[7] T.V.W. Janssens, B.S. Clausen, B. Hvolbak, H. Falsig, C.H. Christensen, T. Bligaard, J.K. Norskov, Top. Catal. 44 (2007) 15.
[8] F. Crdenas-Lizana, S. Gmez-Quero, M.A. Keane, ChemSusChem 1 (2008) 215.
[9] A. Corma, P. Serna, H. Garcia, J. Am. Chem. Soc. 129 (2007) 6358.
[10] K. Shimizu, Y. Miyamoto, T. Kawasaki, T. Tanji, Y. Tai, A. Satsuma, J. Phys. Chem. C 113 (2009) 17803.
[11] A. Corma, P. Serna, Science 313 (2006) 332.
[12] A. Corma, P. Concepción, P. Serna, Angew. Chem. Int. Ed. 46 (2007) 7266.
[13] M. Boronat, A. Concepcin, A. Corma, S. Gonzlez, F. Illas, P. Serna, J. Am. Chem. Soc. 129 (2007) 16230.
[14] M. Boronat, F. Illas, A. Corma, J. Phys. Chem. A 113 (2009) 3750.
[15] T. Sun, K. Seff, Chem. Rev. 94 (1994) 858.
[16] P. Claus, H. Hofmeister, J. Phys. Chem. B. 103 (1999) 2766.
[17] W. Grunert, A. Bruckner, H. Hofmeister, P. Claus, J. Phys. Chem. B 108 (2004) 5709.
[18] M. Bron, D. Teschner, A. Knop-Gericke, B. Steinhauer, A. Scheybal, M. Havecker, D. Wang, R. Fodisch, D. Honicke, A. Wootsch, R. Schlögl, P. Claus, J. Catal. 234 (2005) 37.
[19] M. Bron, D. Teschner, A. Knop-Gericke, F.C. Jentoft, J. Krohnert, J. Hohmeyer, C. Volckmar, B. Steinhauer, R. Schlögl, P. Claus, Phys. Chem. Chem. Phys. 9 (2007) 3559.
[20] M. Steffan, A. Jakob, P. Claus, H. Lang, Catal. Commun. 10 (2009) 437.
[21] Y. Chen, C. Wang, H. Liu, J. Qiu, X. Bao, Chem. Commun. (2005) 5298.
[22] H. Zhang, Q. Fu, Y. Yao, Z. Zhang, T. Ma, D. Tan, X. Bao, Langmuir 24 (2008) 10874.
[23] M. Kreich, P. Claus, Angew. Chem. Int. Ed. 44 (2005) 7800.
[24] P.G.N. Mertens, F. Cuypers, P. Vandezande, X. Ye, F. Verpoort, I.F.J. Vankelecom, D.E. De Vos, Appl. Catal. A 325 (2007) 130.
[25] H. Imamura, K. Fujita, Y. Sakata, S. Tsuchiya, Catal. Today 28 (1996) 231.
[26] Y. Shiraishi, N.J. Toshima, J. Mol. Catal. A 141 (1999) 187.
[27] K. Shimizu, M. Tsuzuki, K. Kato, S. Yokota, K. Okumura, A. Satsuma, J. Phys. Chem. C 111 (2007) 950.
[28] K. Shimizu, K. Sugino, A. Satsuma, Chem. Eur. J. 15 (2009) 2341.
[29] K. Shimizu, R. Sato, A. Satsuma, Angew. Chem. Int. Ed. 48 (2009) 3982.
[30] K. Shimizu, K. Ohshima, A. Satsuma, Chem. Eur. J. 15 (2009) 9977.
[31] K. Shimizu, M. Nishimura, A. Satsuma, ChemCatChem 1 (2009) 497.
[32] T. Mitsudome, Y. Mikami, H. Funai, T. Mizugaki, K. Jitsukawa, K. Kaneda, Angew. Chem. Int. Ed. 47 (2008) 138.
[33] T. Mitsudome, S. Arita, H. Mori, T. Mizugaki, K. Jitsukawa, K. Kaneda, Angew. Chem. Int. Ed. 47 (2008) 7938.
[34] M.J. Beier, T.W. Hansen, J.-D. Grunwaldt, J. Catal. 266 (2009) 320.
[35] B. Hammer, J.K. Norskov, Surf. Sci. 343 (1995) 211.
[36] A.B. Mohammad, I.V. Yudanov, K.H. Lim, K.M. Neyman, N. Rsch, J. Phys. Chem. C 112 (2008) 1628.
[37] A. Montoya, A. Schlunke, B.S. Haynes, J. Phys. Chem. B 110 (2006) 17145.
[38] H.U. Blaser, H. Steiner, M. Studer, ChemCatChem 1 (2009) 210.

[39] M. Suchy, P. Winternitz, M. Zeller, World (WO) Patent 91/00278, 1991.
[40] F. Kovar, F.E. Armond, US Patent 3975,444, 1976.
[41] J. Butera, J. DXC GT, WO Patent 91/09023, 1991.
[42] A. Burawoy, J.P. Critchley, Tetrahedron 5 (1959) 340.
[43] M. Studer, S. Neto, H.-U. Blaser, Top. Catal. 13 (2000) 205.
[44] S. Xu, X. Xi, J. Shi, S. Cao, J. Mol. Catal. A 160 (2000) 287.
[45] M. Takasaki, Y. Motoyama, K. Higashi, S.-H. Yoon, I. Mochida, H. Nagashima, Org. Lett. 10 (2008) 1601.
[46] M.L. Kantam, R. Chakravarti, U. Pal, B. Sreedhar, S. Bhargava, Adv. Synth. Catal. 350 (2008) 822.
[47] A. Corma, P. Serna, P. Concepcion, J.J. Calvino, J. Am. Chem. Soc. 130 (2008) 8748.
[48] P.M. Reis, B. Royo, Tetrahedron Lett. 50 (2009) 949.
[49] B. Coq, A. Tijani, R. Dutartre, F. Figueras, J. Mol. Catal. 79 (1993) 253.
[50] A. Jentys, Phys. Chem. Chem. Phys. 1 (1999) 4059.
[51] Y. Yazawa, H. Yoshida, S. Komai, T. Hattori, Appl. Catal. A 233 (2002) 113.
[52] E.A. Gelder, S.D. Jackson, C.M. Lok, Chem. Commun. (2005) 522.
[53] (a) R. Noyori, T. Ohkuma, Angew. Chem. Int. Ed. 40 (2001) 40;
(b) R.M. Bullock, Chem. Eur. J. 10 (2004) 2366.
[54] T. Shishido, H. Hattori, Appl. Catal. A 146 (1996) 157.